Transverse circular-polarized Bessel beam generation by inward cylindrical aperture distribution

S. C. Pavone,[1,*] **M. Ettorre,**[2] **M. Casaletti,**[3] **and M. Albani**[1]

[1]*Dipartimento di Ingegneria dell'Informazione e Scienze Matematiche, Universit`a di Siena, via Roma 56, 53100 Siena, Italy*

[2]*Institut d'Electronique et de Te´le´communications de Rennes, UMR CNRS 6164, Universite´ de Rennes 1, 35042 Rennes Cedex, France*

[3]*Laboratoire d'Electronique et Electromagne´tisme, Universite´ Pierre et Marie Curie - Paris 6, 75005 Paris, France*

[*]*santi.pavone@unisi.it*

Abstract: In this paper the focusing capability of a radiating aperture implementing an inward cylindrical traveling wave tangential electric field distribution directed along a fixed polarization unit vector is investigated. In particular, it is shown that such an aperture distribution generates a non-diffractive Bessel beam whose transverse component (with respect to the normal of the radiating aperture) of the electric field takes the form of a zero-th order Bessel function. As a practical implementation of the theoretical analysis, a circular-polarized Bessel beam launcher, made by a radial parallel plate waveguide loaded with several slot pairs, arranged on a spiral pattern, is designed and optimized. The proposed launcher performance agrees with the theoretical model and exhibits an excellent polarization purity.

OCIS codes: (050.1220) Apertures; (050.1960) Diffraction Theory; (050.5500) Propagation.

References and links

1. J. Durnin, "Exact solutions for nondiffracting beams. I. The scalar theory," J. Opt. Soc. Am. A **4**, 651–654, (1987).
2. M. R. Lapointe, "Review of non-diffracting Bessel beam experiments," Opt. Las. Tech. **24**, 315, (1992).
3. Z. Li, K. B. Alici, H. Caglayan, and E. Ozbay, "Generation of an axially asymmetric Bessel-like beam from a metallic subwavelength aperture," Phys. Rev. Lett. **102**, (2009).
4. J. Arlt and K. Dholakia, "Generation of high-order Bessel beams by use of an axicon," Opt. Commun., **177**, 297–301, (2000).
5. R. M. Herman and T. A. Wiggins, "Production and uses of diffractionless beams," J. Opt. Soc. Am. A **8**, 932–942, (1991).
6. S. Chávez-Cerda,"A new approach to Bessel beams," J. Mod. Opt. **46**, 923–930, (1999).
7. M. Ettorre and A. Grbic, "Generation of propagating Bessel beams using leaky-wave modes," IEEE Trans. Antennas Propag. **60**, 3605–3613, (2012).
8. H. E. Hernandez-Figueroa, M. Zamboni-Rached, and E. Recami, *Localized Waves*, John Wiley & Sons, **194**, (2007).
9. H. E. Hernandez-Figueroa, M. Zamboni-Rached, and E. Recami, *Nondiffracting Waves*, John Wiley & Sons, (2013).
10. A. Mazzinghi, M. Balma, D. Devona, G. Guarnieri, G. Mauriello, M. Albani, and A. Freni, "Large Depth of Field Pseudo-Bessel Beam Generation with a RLSA Antenna," IEEE Trans. Antennas Propag. **62**, 3911–3919, (2014).
11. M. Ettorre, S. C. Pavone, M. Casaletti, and M. Albani, "Experimental Validation of Bessel Beam generation by using an inward Hankel aperture distribution," IEEE Trans. Antennas Propag. **63**, 2539–2544, (2015).

#257505 Received 15 Jan 2016; revised 1 Apr 2016; accepted 4 Apr 2016; published 12 May 2016

12. S. C. Pavone, M. Ettorre, and M. Albani, "Analysis and Design of Bessel Beam launchers: Longitudinal Polarization," IEEE Trans. Antennas Propag., to be published.
13. M. Albani, S. C. Pavone, M. Casaletti, and M. Ettorre, "Generation of non-diffractive Bessel beams by inward cylindrical traveling wave aperture distribution," Opt. Expr. **22**, 18354–18364, (2014).
14. Z. Bouchal and M. Olivik, "Non-diffractive vector Bessel beams", Journ. Mod. Opt., **42**, 8, 1555–1566, (1995).
15. R. Cicchetti and A. Faraone, "Incomplete Hankel and modified Bessel functions: a class of special functions for electromagnetics," IEEE Trans. Antennas Propag. **52**, 3373–3389, (2004).
16. M. Albani, A. Mazzinghi, and A. Freni, "Automatic design of CP-RLSA antennas," IEEE Trans. Antennas Propag. **60**, 5538–5547, (2012).
17. L. Felsen and N. Marcuvitz, *Radiation and Scattering of Waves*, chap. 5, Prentice-Hall, (1972).
18. M. Casaletti, R. Sauleau, M. Ettorre, and S. Maci, "Efficient Analysis of Metallic and Dielectric Posts in Parallel-Plate Waveguide Structures," IEEE Trans. Microw. Theory Tech. **60**, 2979–2989, (2012).
19. C. Balanis, *Advanced Engineering Electromagnetics*, John Wiley & Sons, (2012).

1. Introduction

In recent years growing interest has been gained by the so-called diffractionless beams, among which Bessel beams assume a relevant importance, since their early introduction by Durnin [1]. On the other hand, several attempts have been made to practically generate Bessel beams [2, 3], both at optical frequencies [4, 5, 6] and at radio frequencies [7, 8, 9].

Whereas Bessel beam launchers usually adopt a standing wave (Bessel function) aperture distribution [10], in [11, 12, 13] it has been shown that Bessel beams can be alternatively generated synthesizing an inward cylindrical traveling wave (Hankel functions) aperture distribution. Namely, in [13] a tangential electric field polarized along the radial unit vector $\hat{\rho}$ and shaped as an inward cylindrical traveling wave $H_1^{(1)}(k_{\rho a}\rho)$ produces a Bessel beam with the longitudinal component (i.e. normal to the radiating aperture) of the electric field shaped as $J_0(k_{\rho a}\rho)e^{-jk_{za}z}$, in a well-defined conical region centered on the axis of symmetry of the radiating aperture. With reference to [14], the excited vector Bessel beam is the $\mathbf{N}_0$ TM vector wave function.

In this paper, we extend the results obtained in [13], showing that a tangential electric field aperture distribution polarized along a fixed unit vector $\hat{\mathbf{p}}$ generates a Bessel beam with the same arbitrary transverse polarization $\hat{\mathbf{p}}$. Again, with reference to [14], the excited vector Bessel beam is a proper superposition of $\mathbf{M}_{\pm 1}$ and $\mathbf{N}_{\pm 1}$ vector wave functions (see example 4 in [14] for vector Bessel beam linearly polarized along $\hat{\mathbf{p}} = \hat{\mathbf{x}}$).

As in [13], the electromagnetic field radiated by an infinite aperture is calculated in a closed form and split in its Geometrical Optics (GO) and Space Wave (SW) contributions, that is written in closed form in terms of the incomplete Hankel functions [15] and can be asymptotically interpreted as a space wave arising from the aperture center. In addition, the case of finite radiating aperture is analyzed numerically, showing that the finiteness of the aperture implies a maximum non-diffractive range, beyond which the Bessel beam starts diffracting.

Finally, to implement a circular-polarized (CP) Bessel beam launcher with a transverse inward cylindrical traveling wave equivalent aperture distribution, a radial parallel plate waveguide (PPW) loaded with several slot pairs arranged on a spiral is designed and optimized. The slot pairs are orthogonally located and excited in quadrature [16], thus allowing the generation of a circular-polarized field.

The presented low profile launcher can profitably find practical application in the field of medical imaging and of ground penetrating radars (GPR), both at millimeter waves and at Terahertz.

2. Analytical formulation for infinite apertures

The geometry of the problem is shown in Fig. 1. An inward cylindrical traveling wave is assumed for the tangential electric field distribution over the radiating aperture $\mathbf{E}_t(\rho, z = 0) =$

#257505 Received 15 Jan 2016; revised 1 Apr 2016; accepted 4 Apr 2016; published 12 May 2016

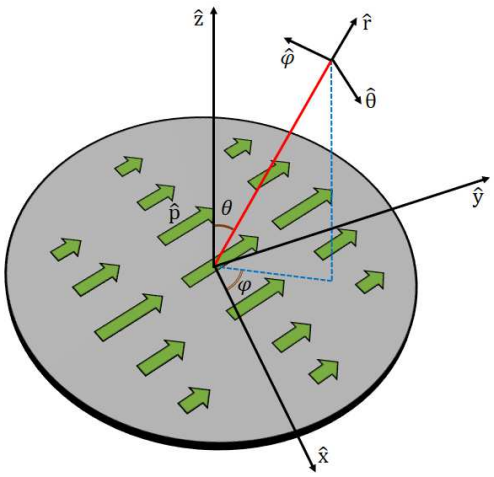

Fig. 1. Pictorial representation of a tangential field distribution directed along a fixed $\hat{\mathbf{p}}$ unit vector. The reference system for the subsequent formulation is highlighted.

$E_t(\rho, z=0)\hat{\mathbf{p}}$, where $\hat{\mathbf{p}}$ is a complex unit vector identifying a generic polarization state, namely linear, circular or elliptical. A time dependence $e^{j\omega t}$, $\omega = 2\pi f$ being the angular frequency, is assumed and suppressed. The electric field radiated by such a tangential electric field aperture distribution [17] at the observation point $\mathbf{r} = \boldsymbol{\rho} + z\hat{\mathbf{z}}$, with $\boldsymbol{\rho} = \rho\hat{\boldsymbol{\rho}} = \rho(\cos\phi\hat{\mathbf{x}} + \sin\phi\hat{\mathbf{y}})$, is

$$\mathbf{E}(\rho, z) = \frac{1}{4\pi}\int_{\infty e^{-j\pi}}^{+\infty} \tilde{E}_t(k_\rho)\left[H_0^{(2)}(k_\rho\rho)\hat{\mathbf{p}} + j\frac{k_\rho}{k_z}H_1^{(2)}(k_\rho\rho)(\hat{\boldsymbol{\rho}}\cdot\hat{\mathbf{p}})\hat{\mathbf{z}}\right]e^{-jk_z z}k_\rho dk_\rho, \tag{1}$$

$$\tilde{E}_t(k_\rho) = 2\pi\int_0^{+\infty} E_t(\rho, z=0)J_0(k_\rho\rho)\rho d\rho, \tag{2}$$

where k is the free-space wavenumber, k_ρ and $k_z = \sqrt{k^2 - k_\rho^2}$ are the radial and the longitudinal spectral variables, whereas $J_n()$ and $H_n^{(m)}()$ are the n-order Bessel and Hankel functions of the m-th kind, respectively. By assuming an inward cylindrical traveling wave aperture distribution $\mathbf{E}_t(\rho, z=0) = H_0^{(1)}(k_{\rho a}\rho)$, with $k_{\rho a} = k\sin\theta_a$ (Fig. 2(a)), its Hankel transform (2) is calculated in closed form as

$$\tilde{E}_t(k_\rho) = -\frac{4j}{k_\rho^2 - k_{\rho a}^2}. \tag{3}$$

By following the analytical procedure outlined in the Appendix, the radiated field is written as the sum of the GO and SW contributions, namely

$$\mathbf{E}(\mathbf{r}) = \mathbf{E}^{GO}(\mathbf{r}) + \mathbf{E}^{SW}(\mathbf{r}), \tag{4}$$

where

$$\begin{aligned}\mathbf{E}^{GO}(\rho, z) = &\left[2J_0(k_{\rho a}\rho)\,\mathrm{U}(\theta_a - \theta) + H_0^{(1)}(k_{\rho a}\rho)\,\mathrm{U}(\theta - \theta_a)\right]e^{-jk_{za}z}\hat{\mathbf{p}}\\ &+ j\frac{k_{\rho a}}{k_{za}}\left[2J_1(k_{\rho a}\rho)\,\mathrm{U}(\theta_a - \theta) + H_1^{(1)}(k_{\rho a}\rho)\,\mathrm{U}(\theta - \theta_a)\right]e^{-jk_{za}z}(\hat{\boldsymbol{\rho}}\cdot\hat{\mathbf{p}})\hat{\mathbf{z}},\end{aligned} \tag{5}$$

#257505 Received 15 Jan 2016; revised 1 Apr 2016; accepted 4 Apr 2016; published 12 May 2016

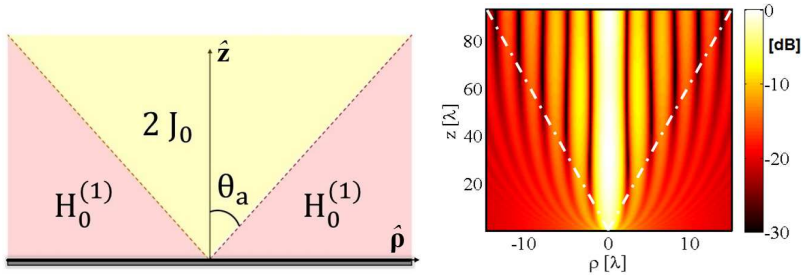

(a) (b)

Fig. 2. (a) Schematic representation of the electric field transverse component, according to the analytical formulation for infinite apertures. In the *yellow* region, a Bessel profile $J_0(k_{\rho a}\rho)$ is achieved in the transverse component of the electric field ($\theta < \theta_a$), whereas in the *red* regions an inward cylindrical traveling wave aperture distribution is present. (b) Map of the magnitude of the transverse component of the electric field in a vertical plane orthogonal to the radiating aperture.

and

$$\begin{aligned}\mathbf{E}^{SW}(\mathbf{r}) &= \left[H_0^{(2)}(k_{\rho a}\rho, w_0^+)e^{jk_{za}z} + \mathrm{sgn}(w_0^-)H_0^{(2)}(k_{\rho a}\rho, |w_0^-|)e^{-jk_{za}z}\right]\hat{\mathbf{p}} \\ &- j\frac{k_{\rho a}}{k_{za}}\left[\mathrm{sgn}(w_0^-)H_1^{(2)}(k_{\rho a}\rho, |w_0^-|)e^{-jk_{za}z} - H_1^{(2)}(k_{\rho a}\rho, w_0^+)e^{jk_{za}z}\right](\hat{\boldsymbol{\rho}}\cdot\hat{\mathbf{p}})\hat{\mathbf{z}} \\ &\sim \frac{2}{\pi k}\frac{1}{\cos^2\theta_a - \cos^2\theta}\frac{e^{-jkr}}{r}\hat{\mathbf{r}}\times(\hat{\mathbf{p}}\times\hat{\mathbf{z}}),\end{aligned} \tag{6}$$

in which $\hat{\mathbf{r}} = \sin\theta\cos\phi\hat{\mathbf{x}} + \sin\theta\sin\phi\hat{\mathbf{y}} + \cos\theta\hat{\mathbf{z}}$, $k_{za} = \sqrt{k^2 - k_{\rho a}^2} = k\cos\theta_a$, $H_m^{(n)}(\Omega, w_0)$ are the m-th order, n-th kind incomplete Hankel functions [15], $w_0^{\pm} = \tanh^{-1}\cos\theta \pm \tanh^{-1}\cos\theta_a$, and $U(\cdot)$ denotes the unit step function.

The GO field comprises a longitudinal ($\hat{\mathbf{p}}$) and a transverse ($\hat{\mathbf{z}}$) part, showing that an infinite aperture is able to generate a non-diffractive Bessel beam with the transverse component of the electric field shaped as a zero-th order Bessel beam in the region $\theta < \theta_a$ around the z-axis (Fig. 2(a)). The SW contribution is also written in a closed-form by means of the incomplete Hankel functions, as in [13, 15], and its asymptotic evaluation reveals that it behaves as a spherical wave with an elevation pattern. On the shadow boundary ($\theta = \theta_a$) the non-uniform asymptotic evaluation fails, thus predicting a diverging field, whereas the exact expression provides the correct transitional behaviour of the SW. It is worth noting that, as revealed by its asymptotic expression, the SW contribution to the field decays as $1/r$ moving far from the radiating aperture, thus the most significant term at a sufficiently large distance from the aperture is the GO contribution. Figure 2(b) shows the magnitude of the transverse $\hat{\mathbf{p}}$-component of the electric field calculated accordingly to (5)–(6) for $f = 60$GHz and $\theta_a = 10^\circ$.

It is worth noting that once the polarization state $\hat{\mathbf{p}}$ is defined, similar results for the radiated field can be achieved using the vector approach proposed in [14]. However, such approach requires a combination of cylindrical modes to generate a defined Bessel beam. The proposed technique only requires an inward cylindrical aperture field distribution to generate arbitrary polarized Bessel beams.

In the next Section, the extension to the case of finite radiating aperture is discussed numerically.

#257505 Received 15 Jan 2016; revised 1 Apr 2016; accepted 4 Apr 2016; published 12 May 2016

3. Numerical field evaluation for finite apertures

The radiation of a finite inward cylindrical aperture distribution has been treated numerically as in [13]. The Hankel transform of the tangential electric field aperture distribution becomes

$$\tilde{E}_t(k_\rho) = -\frac{2}{k_\rho^2 - k_{\rho a}^2}\left[2j + \pi k_{\rho a} a H_1^{(1)}(k_{\rho a}a) J_0(k_\rho a) - \pi k_\rho a H_0^{(1)}(k_\rho a) J_1(k_\rho a)\right], \tag{7}$$

in which a is the radius of the radiating aperture.

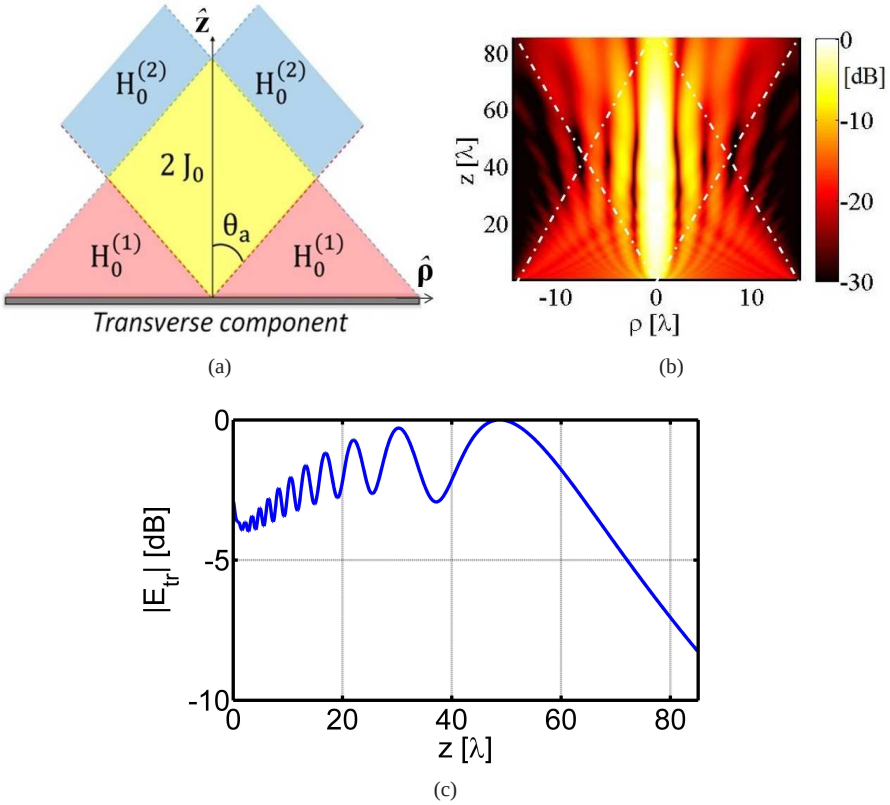

Fig. 3. (a) Schematic illustration of the transverse component of the electric field radiated by a finite aperture implementing an inward cylindrical traveling wave distribution. In the central *yellow* region, the Bessel beam is generated, whereas in the *red* (resp. *blue*) regions an inward (resp. outward) cylindrical traveling wave is present. (b) Map of the magnitude of the transverse component of the electric field in a vertical plane orthogonal to the radiating aperture, obtained by evaluating numerically the integral (1), in which the expression of the tangential electric field aperture distribution for finite apertures (7) is used. (c) Magnitude of the transverse component of the electric field on the longitudinal z-axis at $\rho = 0$.

The electromagnetic field radiated by such a distribution can be calculated by the numerical evaluation of the integral in (1). In Fig. 3(a) the transverse component of the electric field is schematically depicted for the case of a finite radiating aperture with radius $a = 15\lambda$ at the operating frequency $f = 60$GHz, by imposing $\theta_a = 10^\circ$, then $k_{\rho a} = k \sin\theta_a \sim 0.17k$. Figure 3(b) provides the numerical evaluation of the radiated field for the same aperture.

#257505 Received 15 Jan 2016; revised 1 Apr 2016; accepted 4 Apr 2016; published 12 May 2016

As in [13], the Bessel beam is established inside the highlighted region close to the aperture axis of symmetry up to a finite distance, called non-diffractive range, namely $NDR = a\cot\theta_a \sim 85\lambda$. Beyond that distance the beam starts spreading out, thus the assumption of diffractionless Bessel beam is no more valid.

It is worth noting that on the longitudinal z-axis ($\rho = 0$), the field amplitude oscillates, as clear from Fig. 3(c). Such a phenomenon is due to the finiteness of the radiating aperture and consequent on-axis interference of the diffracted rays from the aperture rim.

4. Implementation of a circular-polarized Bessel beam launcher

In this Section, a practical implementation of a circular-polarized Bessel beam launcher is presented. A radial parallel-plate waveguide (PPW) filled with a foam of relative dielectric permit-

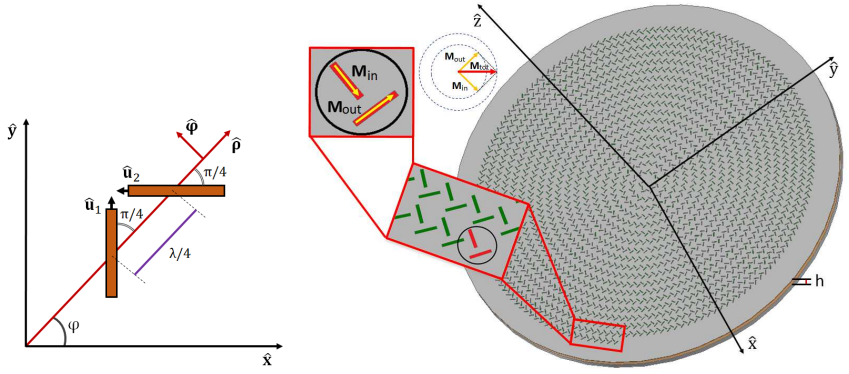

Fig. 4. (a) Pair of radiating slots, generating a circular-polarized field. (b) Pictorial illustration of the radial PPW loaded with several slot pairs generating a circular-polarized radiated field. The geometry of the each slot pair is highlighted and the total equivalent magnetic dipole moment of the slots $\mathbf{M}_{tot}(\rho,\phi) = \mathbf{M}_{in}(\rho,\phi) + \mathbf{M}_{out}(\rho,\phi)$ is graphically shown.

tivity $\varepsilon_r = 1.04$ and thickness $h = 1.575$mm, loaded with several radiating slot pairs has been designed in order to synthesize an inward cylindrical wave aperture distribution of the form $\mathbf{E}_t(\rho, z=0) = H_0^{(1)}(k_{\rho a}\rho)\hat{\mathbf{p}}$, with $\hat{\mathbf{p}} = (\hat{\mathbf{x}} - j\hat{\mathbf{y}})/\sqrt{2}$ denoting the right-handed circular polarization (RHCP) unit vector. The excited vector Bessel beam polarization is in turn a RHCP, and its expansion in terms of vector wave functions [14] comprises a superposition of the $\mathbf{M}_1$ and $\mathbf{N}_1$; namely the expansion coefficients of (3) of [14] are $\alpha_n^{(+)} = \alpha\delta_{n1}$ and $\alpha_n^{(-)} = 0$, with δ_{nm} denoting the Kronecker symbol and α an arbitrary amplitude. Each pair comprises two orthogonal slots (making an angle of $\pm 45^\circ$ with respect to the radial direction), which are $\lambda_d/4 = \lambda_0/(4\sqrt{\varepsilon_r})$ apart to be fed in quadrature by the outward feeding wave in the PPW, thus radiating a RHCP (Fig. 4(a)). In addition, the slots are arranged along a spiral to recreate the same phase profile of the target inward traveling wave aperture distribution (Fig. 4(b)). The design parameters are those used in Sec. 3 for the numerical analysis of finite radiating devices.

The optimization technique developed in [16] and profitably used in [13], together with an in-house Method of Moments for the analysis of the electromagnetic field distribution [18] have been used to synthesize the focusing system.

The co-polar component (RHCP) of the electric field is presented together with its cross-polar component (LHCP), both in the $\rho - z$ plane (Fig. 5(a)-(b)) and in the transverse $x - y$ plane at $z = NDR/2 = 42.5\lambda$ (Fig. 5(c)-(d)), showing an excellent polarization purity of the

#257505 Received 15 Jan 2016; revised 1 Apr 2016; accepted 4 Apr 2016; published 12 May 2016

launcher. By comparing Fig. 5(a) to Fig. 3(b), a clear consistency between the synthesized field and the theoretical model is revealed.

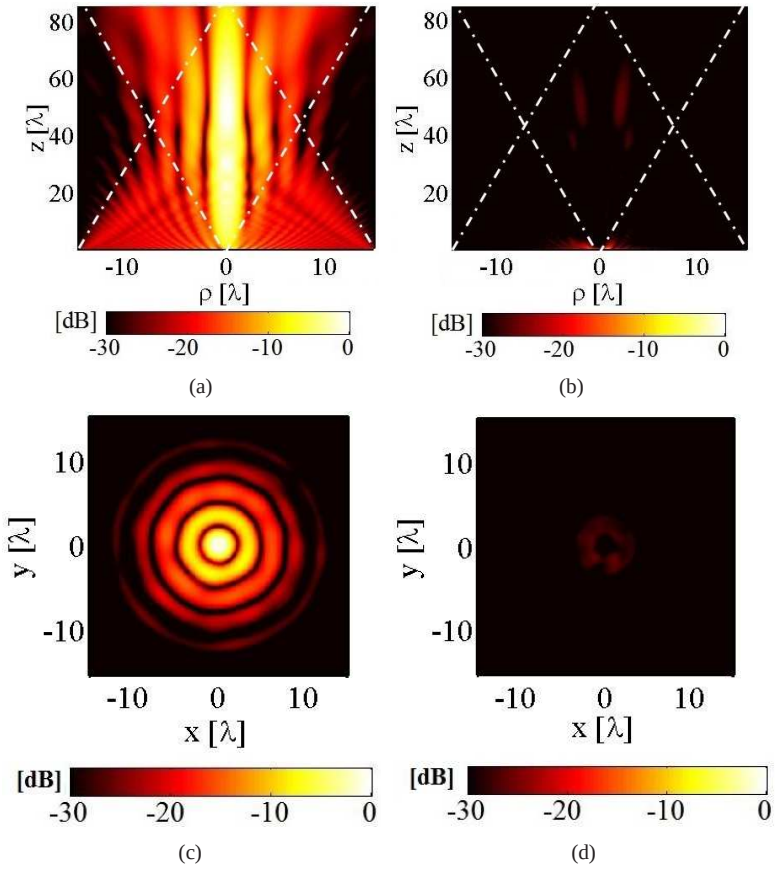

Fig. 5. (a,c) Co-polar (RHCP) and (b,d) cross-polar (LHCP) components of the electric field radiated by the designed focusing system, evaluated in the $\rho - z$ (a,b) and $x - y$ (c,d) planes at $z = NDR/2$. The cross-polar component is almost everywhere less than -20dB, demonstrating a good rejection of the undesired cross-polarization.

5. Conclusion

In this paper, the capability of an inward cylindrical traveling wave aperture distribution directed along a fixed unit vector $\hat{\mathbf{p}}$ to generate a non-diffractive Bessel beam in the transverse component of the electric field has been demonstrated. Moving from the analytical formulation for an infinite radiating aperture, the electromagnetic field has been split into the GO and SW contributions, showing that the SW contribution can be written in a closed form by using the definition of the incomplete Hankel functions and asymptotically reveals its spherical wave nature. Moreover, the analytical model for infinite apertures has been extended numerically to the case of finite radiating aperture. In the second part, a CP Bessel beam launcher has been designed and optimized. The achieved results clearly show a nice agreement with the theoretical analysis and a remarkable polarization purity.

#257505 Received 15 Jan 2016; revised 1 Apr 2016; accepted 4 Apr 2016; published 12 May 2016

Appendix

By using the vector potential $\mathbf{F}(\mathbf{r})$, according to its definition [19], the electric field can be calculated by differentiation as

$$\mathbf{E}(\mathbf{r}) = -\frac{1}{\varepsilon}\nabla \times \mathbf{F}(\mathbf{r}), \tag{8}$$

where

$$\mathbf{F}(\mathbf{r}) = \varepsilon \iint_{slots} \mathbf{E}(\mathbf{r}') \times \hat{\mathbf{z}} \frac{e^{-jkR}}{2\pi R} dS', \tag{9}$$

in which $R = |\mathbf{r} - \mathbf{r}'|$ is the distance between the source and the observation point.

The integral in (9) is the convolution of the tangential electric field and the scalar Green's function for an unbounded semi-infinite medium. In the spectral domain, (1) can be written as ($z > 0$)

$$\mathbf{F}(\mathbf{r}) = \frac{\varepsilon}{4\pi j}\hat{\mathbf{p}} \int_{\infty e^{-j\pi}}^{+\infty} \tilde{E}_t(k_\rho) H_0^{(2)}(k_\rho \rho) \frac{e^{-jk_z z}}{k_z} k_\rho dk_\rho, \tag{10}$$

that can be related to the scalar potential $S(\mathbf{r})$ introduced in [13] by the relation $\mathbf{F}(\mathbf{r}) = \varepsilon k_{\rho a} S(\mathbf{r})(\hat{\mathbf{p}} \times \hat{\mathbf{z}})$, therefore the GO and SW contributions of the potential can be easily calculated by following the Appendix of [13] as

$$\mathbf{F}^{GO}(\mathbf{r}) = \frac{\varepsilon}{jk_{za}} e^{-jk_{za}z} \left[2J_0(k_{\rho a}\rho)\,\mathrm{U}(\theta_a - \theta) + H_0^{(1)}(k_{\rho a}\rho)\,\mathrm{U}(\theta - \theta_a) \right] (\hat{\mathbf{p}} \times \hat{\mathbf{z}}),$$

and

$$\mathbf{F}^{SW}(\mathbf{r}) = \frac{\varepsilon}{jk_{za}} \left[H_0^{(2)}\left(k_{\rho a}\rho, w_0^+\right) e^{jk_{za}z} - \mathrm{sgn}(w_0^-) H_0^{(2)}\left(k_{\rho a}\rho, |w_0^-|\right) e^{-jk_{za}z} \right] (\hat{\mathbf{p}} \times \hat{\mathbf{z}}).$$

According to (8), the GO contribution to the electric field can be determined by differentiation, thus

$$\begin{aligned} \mathbf{E}^{GO}(\rho, z) = & \left[2J_0(k_{\rho a}\rho)\,\mathrm{U}(\theta_a - \theta) + H_0^{(1)}(k_{\rho a}\rho)\,\mathrm{U}(\theta - \theta_a) \right] e^{-jk_{za}z} \hat{\mathbf{p}} \\ & + j\frac{k_{\rho a}}{k_{za}} \left[2J_1(k_{\rho a}\rho)\,\mathrm{U}(\theta_a - \theta) + H_1^{(1)}(k_{\rho a}\rho)\,\mathrm{U}(\theta - \theta_a) \right] e^{-jk_{za}z} (\hat{\boldsymbol{\rho}} \cdot \hat{\mathbf{p}}) \hat{\mathbf{z}}, \end{aligned} \tag{11}$$

whereas the SW contribution is

$$\begin{aligned} \mathbf{E}^{SW}(\mathbf{r}) = & \left[H_0^{(2)}(k_{\rho a}\rho, w_0^+) e^{jk_{za}z} + \mathrm{sgn}(w_0^-) H_0^{(2)}(k_{\rho a}\rho, |w_0^-|) e^{-jk_{za}z} \right] \hat{\mathbf{p}} \\ & - j\frac{k_{\rho a}}{k_{za}} \left[\mathrm{sgn}(w_0^-) H_1^{(2)}(k_{\rho a}\rho, |w_0^-|) e^{-jk_{za}z} - H_1^{(2)}(k_{\rho a}\rho, w_0^+) e^{jk_{za}z} \right] (\hat{\boldsymbol{\rho}} \cdot \hat{\mathbf{p}}) \hat{\mathbf{z}} \end{aligned} \tag{12}$$

To highlight the wave nature of the SW contribution to the electric field, the non-uniform asymptotic expansion of the incomplete Hankel functions is provided, namely

$$H_\nu^{(2)}(\Omega, w_0) \sim \frac{e^{j\nu\pi/2}}{\pi} \frac{\cosh \nu w_0}{j\Omega \sinh w_0} e^{-j\Omega \cosh w_0}, \tag{13}$$

from which the SW contribution to the vector potential (11) is asymptotically evaluated as

$$\mathbf{F}^{SW}(\mathbf{r}) \sim \frac{2}{\pi k} \frac{1}{\cos^2\theta_a - \cos^2\theta} \frac{e^{-jkr}}{r} \hat{\mathbf{r}} \times (\hat{\mathbf{p}} \times \hat{\mathbf{r}}), \tag{14}$$

which reveals the spherical wave nature of the space wave contribution of the electric field.

#257505 Received 15 Jan 2016; revised 1 Apr 2016; accepted 4 Apr 2016; published 12 May 2016

Acknowledgments

Mauro Ettorre would like to thank the University of Rennes 1 (Action incitative, projets scientifiques émergents 2016) for its support.

#257505 Received 15 Jan 2016; revised 1 Apr 2016; accepted 4 Apr 2016; published 12 May 2016